

Design and Measurement of a Waveguide Probe Based WR3.4 Optically Controlled Modulator

Jake A. Connors^{1*}, C.-Y. E. Tong², Paul K. Grimes², A. Gebreyohannes³ and Lei Liu⁴

¹Physics Department, Harvard University, Cambridge, MA 02138

²Smithsonian Astrophysical Observatory, Cambridge, MA 02138

³Center for Nanoscale Systems, Harvard University, Cambridge, MA 02138

⁴Electrical Engineering Department, Notre Dame University, Notre Dame, IN 46556

*Contact: jconnors@physics.harvard.edu

Abstract— Presented is the design and measurement of an optically controlled modulator implemented in waveguide at WR3.4. The symmetric device consists of offset input and output waveguides bridged by a microstrip transmission line with radial waveguide probes patterned onto a thin silicon chip. Optical illumination of the chip at photon energies larger than the silicon bandgap generates free charge carriers in the silicon substrate, modulating its conductivity and dielectric constant. This photoconductive effect allows for the modulation of the millimeter-wave loss along the microstrip transmission line. Initial testing of the device has demonstrated up to 40dB of attenuation, with less than 1.5dB insertion loss in the off-state. A modulation bandwidth of 2MHz has been demonstrated, indicating a sub-100ns fall time when operated as a fast switch.

INTRODUCTION

The control and modulation of millimeter-wave source power is crucial to many applications from radar to antenna mapping to network analysis. Mechanically actuated variable attenuators, ferrite modulators or pin-diode attenuators can provide such control, however it comes at the cost of slow modulation speeds, narrow operating bandwidth or poor off-state insertion loss. Optically controlled modulators, however, can provide fast wideband modulation with wide attenuation range and low off-state insertion loss. The implementation of optically controlled devices has varied, from modulators built in dielectric waveguide[1,2] and dielectric loaded metal waveguide [3-5], quasi-optical modulators and beam-formers[6-9], ultrafast switches and programmable attenuators in planar transmission line[10-13], and photonic-bandgap switches[14]. We implement an optically controlled modulator/continuously variable attenuator in WR3.4 (220-330GHz) as a short section of microstrip transmission line bridging offset symmetric input/output waveguides. The microstrip line is terminated on both ends with a radial stub transition to WR3.4 waveguide, allowing modulation of the device insertion loss through optical illumination of the microstrip line where the electric field is concentrated and less frequency dependent than in waveguide.

FABRICATION AND BLOCK DESIGN

As shown in Figure 1, the device consists of a 25 μ m thick silicon chip bridging two offset rectangular waveguides. The



Fig. 1 A view of the microstrip-to-waveguide probe chip as installed in the E-plane split block. Also visible are the WR3.4 waveguides each with a single capacitive tuning step.

chip is patterned with a 50 Ω microstrip transmission line terminated on either end by a single-ended radial stub transition to WR3.4 waveguide[15,16]. The waveguide block, shown in Fig. 2b, was fabricated from Tellurium-Copper as an E-plane split block. A shallow trench in the lower waveguide block contains the probe chip, as seen in Fig. 2a. In the upper waveguide block, an air cavity sits above the microstrip line and constrains the silicon chip to sit within its trench when assembled. The probe chip was fabricated with simple photolithography to define deposition and etch masks, thermal evaporation for Cr/Au deposition and Bosch-process[17] deep reactive ion etching to free the barbell shaped chip from the parent wafer. The dimensions of the probe chip and the cavity above were chosen to make all higher-order and waveguide-like modes in this transmission line evanescent below 330GHz and thus not contribute to the coupling between waveguides. The radial stub transition with a single capacitive tuning step was designed and optimized in ANSYS HFSS[18] to achieve a better than -26 dB return loss across the entire WR3.4 band. With back to back transitions, this results in a better than -20dB device input return loss, which can be seen in the black dotted line of Fig. 3b.

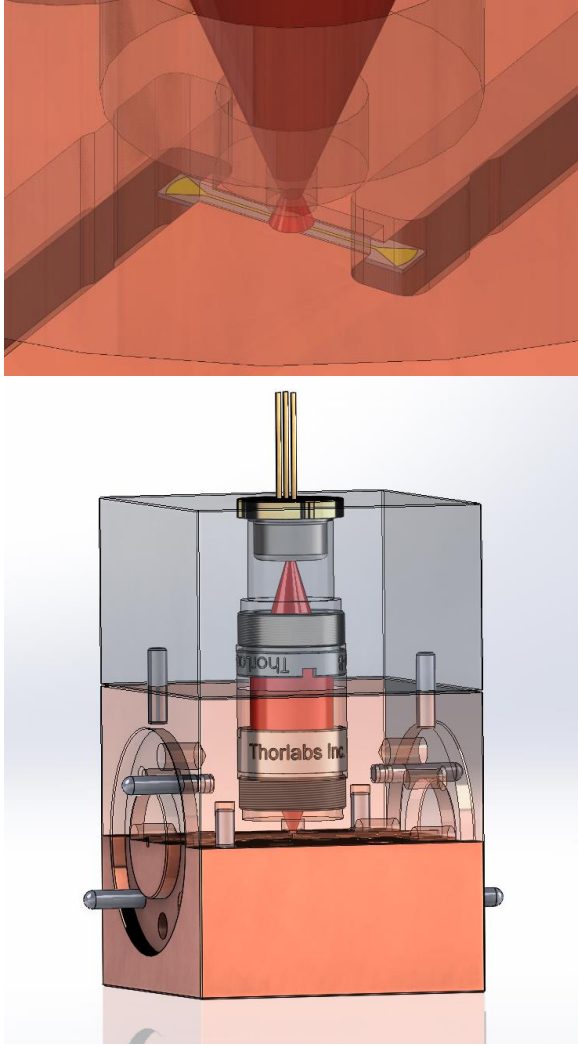


Fig. 2 (Top) View of probe chip as assembled in the waveguide block. Light passes through a small hole in the upper cavity onto the chip. (Bottom) Completed assembly of waveguide split-block and laser diode block. Shown in red is the beam of the 808nm laser diode as collimated and focused by the two-lens system.

Illumination of the probe chip is achieved using a laser diode and two-lens focusing system built into the waveguide and upper laser diode block, as shown in Fig. 2b. An 808nm multimode laser diode with up to 1W continuous output power was used for initial testing. The laser diode wavelength was chosen such that the absorption depth of the light impinging on the silicon chip was approximately half of the chip's thickness. This allows for carrier generation distributed throughout the thickness of the chip while keeping total absorption near 99%, discounting reflection from the air/silicon interface. We operate the laser diode using a current source to provide stable output power and to avoid the effects of thermal runaway in the diode. The laser diode is clamped into place in the upper block, allowing for sufficient alignment and heatsinking. A thread mounted aspheric lens was built into the same block as the laser diode

and serves to collimate the laser diode output. The second aspheric lens, built into the waveguide block, focuses the light through a small aperture leading to the microstrip cavity, where the light can illuminate the center of the probe chip as shown in Fig. 2a. The two blocks are aligned with precision dowels to roughly center the optical beam. Because the optical beam is collimated between the two blocks, the upper block can be replaced with any collimated light source. The position of the lenses were tuned to maximize optical throughput as measured by an optical power meter, achieving nearly 50% coupling of the available optical power to the probe cavity.

DEVICE OPERATING PRINCIPLE

Optical illumination in a concentrated area of the microstrip transmission line modulates the bulk silicon substrate conductivity, leading to loss in the microstrip line. In this way the attenuation of the device can be controlled using the intensity of absorbed optical power. Simulations of the full device insertion loss and return loss are shown in Figure 3, as modelled by HFSS, for varying substrate conductivities. In these models, it is assumed that a 200 μm long section of the microstrip line is illuminated and becomes conductive uniformly through the thickness of the chip. This model predicts that the insertion loss in dB increases nearly

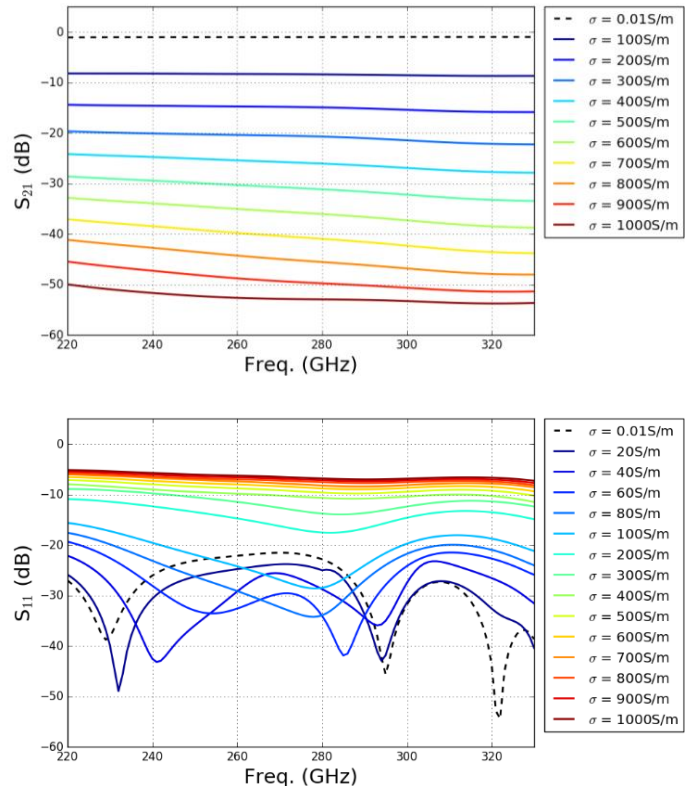


Fig. 3 Insertion loss (top) and return loss (bottom) of the full device as modelled by ANSYS HFSS for varying levels of substrate conductivity. It is assumed that illumination only changes the conductivity over a 200 μm long section of the silicon probe chip.

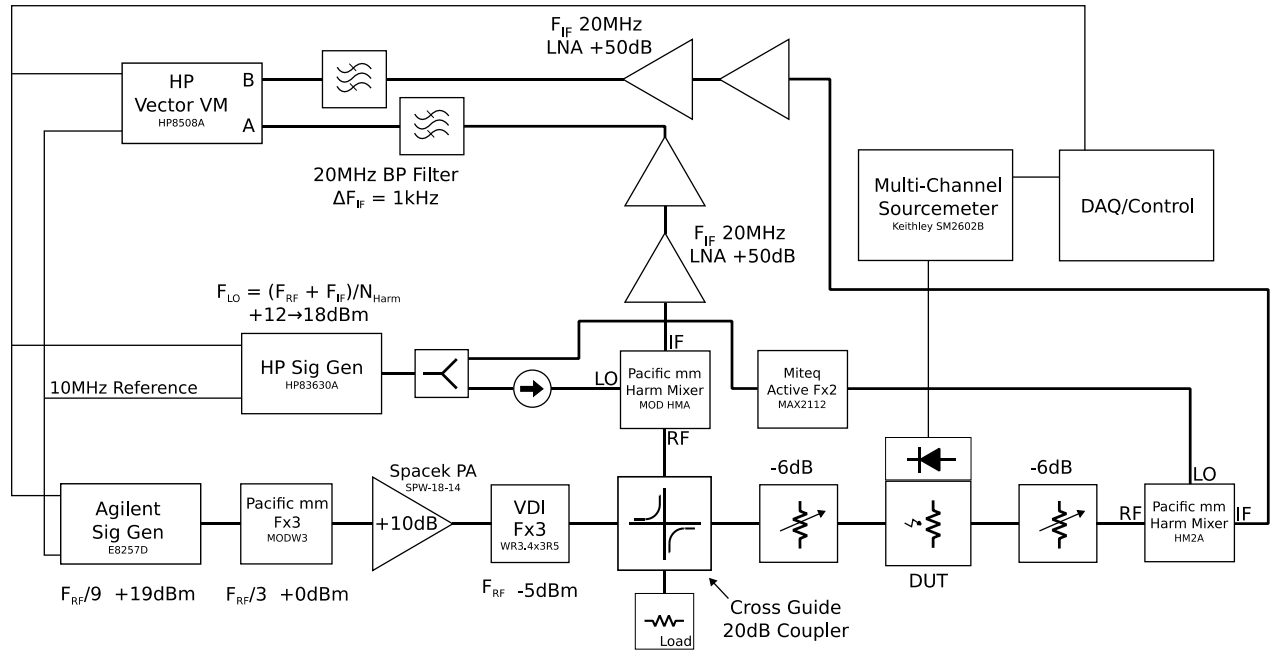


Fig. 4 Schematic of transmission measurement scheme. A coupled portion of the RF signal and the remainder after passing through the DUT are sent through a down-converting and amplification chain to an HP8508A Vector Voltmeter for measurement of the relative amplitude and phase of the transmitted signal.

linearly with substrate conductivity. The input is well matched at low substrate conductivity, but becomes increasingly reflective as the substrate conductivity increases beyond 100S/m.

Photons impinging on a semiconductor with energy larger than the bandgap energy can be absorbed by electrons in the semiconductor valence band, elevating them to the conduction band. The resulting electron-hole pairs are free to move under the influence of electric fields and thus

contribute to the bulk conductivity of the semiconductor, known as the photoconductive effect. In the low frequency Drude limit, the bulk conductivity is given by:

$$\sigma = e(n_e\mu_e + n_h\mu_h) \quad [1]$$

where n_i is the carrier density and μ_i is the mobility for holes or electrons. The equilibrium carrier density under optical illumination is given by:

$$n_i = P_{inc} \frac{\lambda}{hc} \epsilon_{opt} \tau_i \quad [2]$$

where P_{inc} is the incident optical power per unit volume, ϵ_{opt} is the optical coupling efficiency and τ_i is the hole or electron lifetime. In order to maintain a low off-state insertion loss, high-resistivity floatzone silicon was used having a bulk resistivity $> 10^4 \text{ohm-cm}$, implying that the native dopant density and thus the native carrier density is very small. The carrier lifetime is a function of the various recombination mechanisms taking place within the wafer. The primary bulk recombination process at low carrier density, Shockley-Read-Hall recombination[19], occurs on timescales of $\sim 1\text{ms}$ in very pure silicon, such as was used here. Other bulk recombination processes, such as radiative or Auger recombination only contribute at very high carrier densities, which were likely not seen in our testing. Due to the small thickness of chip used, the dominant recombination pathway is surface recombination, which occurs due to the large multiplicity of defect sites at the termination of the

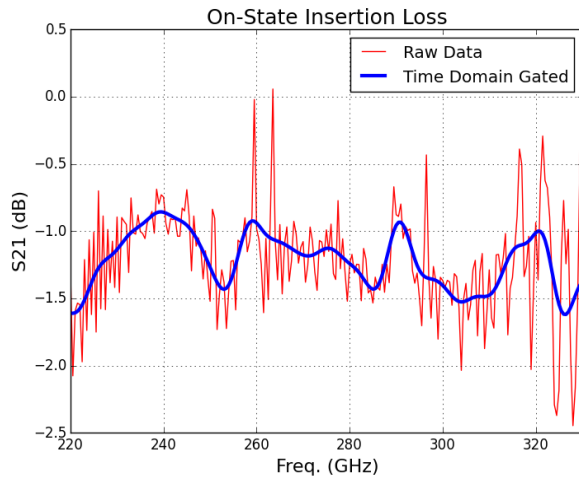


Fig. 5 Measurement of the insertion loss of the device in the no illumination or on-state. Time domain gating was applied to systematically smooth the data.

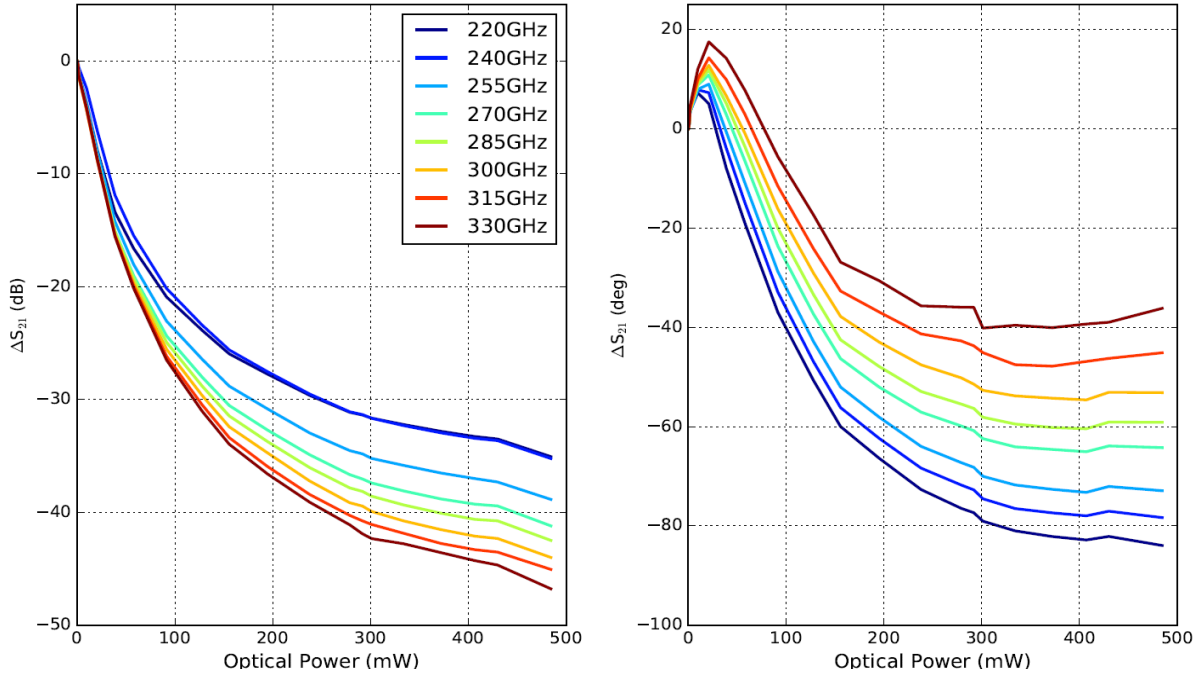


Fig. 6 Measurements of device insertion loss (left) and phase shift (right) versus incident optical power at 808nm for several frequencies across the WR3.4 band. HFSS modelling predicts a linear relationship between conductivity and insertion loss, which is seen for low incident power.

crystal lattice at the surface. The surface recombination time for a wafer with similar surfaces is given by [20,21]:

$$\tau_s = \frac{h}{2s_v} + \frac{h^2}{\pi^2 D} \quad [3]$$

where h is the thickness of the wafer. The first term in Eqn. 3 represents the time necessary for a charge carrier to recombine once it has reached the surface, parameterized by s_v , the surface recombination velocity. This parameter is an empirical measure of the density of surface defects which is dependent upon the exact details of surface preparation and passivation. The second term represents the average time required for a charge carrier to diffuse to the surface, parameterized by D , the carrier diffusion constant. Using the known value for D in silicon at room temperature of $27\text{cm}^2/\text{s}$, the surface lifetime of a $25\mu\text{m}$ thick wafer can be estimated to be at least 24ns, but is ultimately determined by the surface recombination velocity. In the following sections, we therefore do not assume a carrier lifetime, but attempt to estimate it through various measurement techniques.

TRANSMISSION MEASUREMENTS

Measurements of the device were performed in waveguide over the WR3.4 band (220GHz-330GHz) using a coherent source/ receiver setup as shown in Fig. 4. The RF source is an amplifier-multiplier chain driven by a signal at $f_{RF}/9$ producing upwards of -5dBm of power across the WR3.4 band. A cross-guide coupler/harmonic mixer at the output of the RF source allows the amplitude and phase of the RF

signal to be monitored. The signal then passes through the device under test and is detected in a final harmonic mixer. Local oscillator (LO) signals are provided via a power splitter to both harmonic mixers by a common signal generator. The LO harmonic number and power were optimized for each frequency point to maximize the dynamic range of the system. The 20MHz IF signal from both the reference and thru harmonic mixers are then amplified and fed into an HP Vector Voltmeter (VVM) which measures the relative amplitude and phase of the two signals. In the operating regime of our measurement setup, the harmonic mixers, amplifiers and VVM are linear with respect to the RF signal, so the IF signals are both linearly related to their RF counterparts allowing a relative amplitude and phase measurement of the device under test. In the limit that the device under test and harmonic mixers are perfectly matched, the resultant measurement is exactly calibrated by taking a set of reference measurements without the device under test. This is not true in practice, so a set of adjustable-vane attenuators are placed before and after the device under test to improve the system match.

Measurements of the insertion loss of the device without optical illumination are shown in Fig. 5. This measurement was calibrated by taking the ratio of measurements performed with and without the device in the measurement system. The insertion loss varies between 1 and 1.5 dB across the WR3.4 band. Time domain gating was performed using a gate the electrical length of the entire waveguide block to systematically smooth the data.

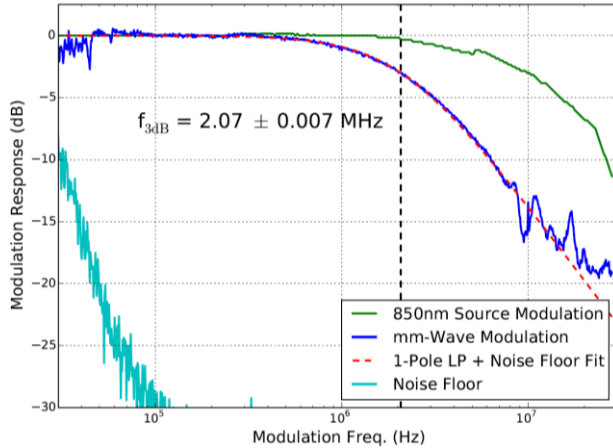


Fig. 7 Measurement of the modulation bandwidth of the device using a 20MHz 5mW IR LED source. A 3dB bandwidth of more than 2MHz is measured corresponding to a ~ 77 ns carrier lifetime.

To measure the insertion loss of the device at varying levels of absorbed optical power, an 808nm laser diode was used to illuminate the device. By varying the current driven into the laser diode, the optical power can be controlled. The incident optical power through the upper portion of the waveguide split block was measured using an optical power meter for varying laser diode currents. Shown in Fig. 6 are measurements of the insertion loss of the device versus incident optical power for various frequencies across the WR3.4 band. The insertion loss is smoothly varying with frequency and monotonically increases with incident optical power. Up to 10dB of attenuation is achieved with incident optical powers of only 20mW, while up to 45dB of attenuation is achieved with an incident optical power of 500mW. While HFSS simulations imply that the insertion loss is a nearly linear function of substrate conductivity, the experimentally realized insertion loss shows diminishing returns at higher incident optical power. This is likely due to significant heating of the substrate by the incident light, causing an increase in temperature and thus lower carrier mobilities and conductivity.

For low incident optical power, where insertion loss is nearly linear with incident power and heating is unimportant, these measurements and the HFSS predictions for the insertion loss can be used to make an estimate of the effective ambipolar carrier lifetime. In making this calculation, the simple relations for Si substrate conductivity in Eqn. 1 and 2 are used to convert from delivered optical power to effective substrate conductivity. In doing so, we assume known carrier mobilities in silicon of $\mu_e \approx 1400 \text{ cm}^2/\text{V} \cdot \text{s}$ and $\mu_h \approx 450 \text{ cm}^2/\text{V} \cdot \text{s}$, an illuminated area of $200\mu\text{m} \times 100\mu\text{m}$, and an optical efficiency of 0.6 due to reflection from the air-Si interface. The illuminated area was chosen to match the calculated optical beam size at the substrate. Using these rough assumptions, a carrier lifetime of approximately 60ns was estimated.

MODULATION BANDWIDTH MEASUREMENT

When used with a fast optical source, our device can operate as a millimeter-wave amplitude modulator. The switching speed or modulation bandwidth of our device is inherently limited by the carrier lifetime in Si. An identical RF source as used in the transmission measurement was used for this measurement. An 850nm IR LED with a 10ns rise and fall time was used as a fast optical source. The LED produced at most 5mW of optical power, of which only a small fraction was coupled onto the device. The millimeter-wave signal transmitted through the device was detected in a harmonic mixer pumped with an LO to produce an IF frequency of 200MHz. Using a spectrum analyzer, the carrier amplitude at 200MHz was compared to the sideband amplitude created by the optical modulation. Shown in Fig. 7 are results of the modulation bandwidth measurement. Results are normalized to the response at low modulation frequency.

As measured, the device exhibits a modulation bandwidth of approximately 2MHz. The modulation bandwidth of the optical source itself was measured to be approximately 10MHz, far enough above the measured bandwidth to be neglected in the estimate of the device bandwidth. Under the assumption that the carrier distribution is near equilibrium at all times, the modulation bandwidth can be calculated in the low-attenuation regime from the effective carrier lifetime as:

$$f_{3dB} = \frac{1}{2\pi\tau_{eff}} \quad [4]$$

where τ_{eff} is the effective carrier lifetime owing to contributions from all recombination pathways. Using this, we measure the effective carrier lifetime to be 76.9 ± 0.3 ns, in agreement with the rough estimate from transmission measurements.

CONCLUSIONS

We have designed and measured a new implementation of an optically controlled waveguide attenuator. Through the use of a back-to-back waveguide probe chip fabricated on thin silicon, up to 40dB of millimeter-wave attenuation was achieved over the entire WR3.4 band, with an off-state insertion loss less than 1.5dB. When operated as a fast modulator, the bandwidth of the device has been measured to be approximately 2MHz, limited by the effective photo-generated carrier lifetime. The device shows promising performance in both dynamic range and modulation bandwidth, suggesting its possible use in millimeter-wave test and measurement systems. Further improvements will be made in two directions. For use as a variable attenuator, we seek to decrease the required optical power per unit attenuation, which can be achieved through anti-reflection coating, surface passivation and heat sinking of the probe chip. For use as a fast modulator, we plan to fabricate similar probe chips out of GaAs, a direct bandgap semiconductor which has a much shorter carrier lifetime, allowing for a vastly larger modulation bandwidth.

REFERENCES

- [1] Chi H. Lee, Paul S. Mak, and A.P. DeFonzo, "Optical Control of Millimeter-Wave Propagation in Dielectric Waveguides," *IEEE Journal of Quantum Electronics*, Vol. QE-16, No. 3, March 1980.
- [2] M. Tsutsumi and A. Alphones, "Optical Control of Millimeter Waves in the Semiconductor Waveguide," *IEICE Trans. On Electronics*, Vol. E76-C, No. 2, pp. 175-182, 1993.
- [3] B. Kazan, "Light-controlled Waveguide Attenuator," US Patent 2856589 A, 14 Oct 1958.
- [4] E. Episkopou, "Reconfigurable optically-controlled waveguide for terahertz application," Ph.D. Thesis, Imperial College London, May 2014.
- [5] Z. Jiang et. al, "Investigation and Demonstration of a WR-4.3 Optically Controlled Waveguide Attenuator," *IEEE Trans. on THz Sci. and Tech*, Vol. 7, No. 1, Jan. 2017.
- [6] S. Biber, D. Schneiderbanger and L.-P. Schmidt, "Design of a Controllable Attenuator with High Dynamic Range for THz-Frequencies based on Optically Stimulated Free Carriers in High-Resistivity Silicon." *Frequenz*, Vol. 59, Iss. 5-6, June 2005.
- [7] S. Lee, Y. Kuga and R.A. Mullen, "Optically Tunable Millimeter-Wave Attenuator Based on Layered Structures," *Microwave and Optical Tech. Lett.*, Vol. 27, No. 1, Oct. 2000.
- [8] L.-J. Cheng and L. Liu, "Optical modulation of continuous terahertz waves towards cost-effective reconfigurable quasi-optical terahertz components," *Optics Express*, Vol. 21, Iss. 23, Nov. 2013.
- [9] T. Gallacher et. al, "Optical Modulation of Millimeter-Wave Beams Using a Semiconductor Substrate," *IEEE Trans. MTT*, Vol. 60, No. 7, July 2012.
- [10] A. Johnson and D. Auston, "Microwave switching by picosecond photoconductivity," *IEEE Journal of Quantum Electronics*, Vol. 11, Iss. 6, June 1975.
- [11] W. Platte, "Optoelectronic Microwave Switching via Laser Induced Plasma Tapers in GaAs Microstrip Sections," *IEEE Trans. MTT*, Vol. MTT-29, No. 10, Oct. 1981.
- [12] R. Kremer et. al, "Optically Controlled Coplanar Transmission Lines for Microwave Signal Processing," *IEEE Trans. MTT*, Vol. 43, No. 9, Sept. 1995.
- [13] S. Lee et. al, "Optically CW-Mode Controlled Microwave Switches with Carrier-Confinement on a Coplanar Waveguide," *IEEE Antennas and Propagation Society Int. Symposium*, July 2001.
- [14] W. Otter et. al, "Photoconductive Photonic Crystal Switch," 2013 38th International Conference on *IRMMW-THz*, Mainz, 2013, pp. 1-2.
- [15] S. Withington, G. Yassin, J. Leech, K.G. Isaak, "An accurate expression for the input impedance of one-sided microstrip probes in waveguide," *Tenth International Symposium on Space Terahertz Technology*, Charlottesville, March 1999.
- [16] J.W. Kooi et. al, "A Full-Height Waveguide to Thin-Film Microstrip Transition with Exceptional RF Bandwidth and Coupling Efficiency," *International Journal of Infrared and Millimeter Waves*, Vol. 24, Iss. 3, pp 261-284, March 2003.
- [17] F. Laermer and A. Schilp of Robert Bosch GmbH, "Method of Anisotropically Etching Silicon," US Patent No. 5501893, 1999.
- [18] Ansoft Corporation, Four Station Square, Suite 200, Pittsburgh, PA 15219-1119, USA
- [19] W. Shockley and W.T. Read, Jr., "Statistics of the Recombinations of Holes and Electrons," *Physical Review*, Vol. 87, No. 5, Sept 1952.
- [20] K.L Luke and L.-J. Cheng, "Analysis of the interaction of a laser pulse with a silicon wafer: Determination of the bulk lifetime and surface recombination velocity," *Journal of Applied Physics*, Vol. 61, No. 6, pp. 2282-2293, March 1987.
- [21] A.B. Sproul, "Dimensionless solution of the equation describing the effect of surface recombination on carrier decay in semiconductors," *Journal of Applied Physics*, Vol. 76, No. 5, pp. 2851-2854, Sept. 1994.